A new 4-D dynamical modeling of the Moon orbital and rotational motion developed at POLAC.

A. Bourgoin, C. Le Poncin-Lafitte, S. Bouquillon, G. Francou, M.-C. Angonin

SYRTE, Observatoire de Paris, PSL Research University, CNRS, Sorbonne Universités, UPMC Univ. Paris 06, LNE, 61 avenue de l'Observatoire, 75014 Paris, France.

Abstract

Nowadays, *General Relativity* (*GR*) is very well tested across the Solar System using observables given by the tracking of spacecraft [3], *Very Long Baseline Interferometry* (*VLBI*) [5] and *Lunar Laser Ranging* (*LLR*) [6]. These tests are mainly computed on two frameworks respectively based on the *Post Parametrized Newtonian* (*PPN*) and the search for a fifth force. Some motivations are given to look for deviations from *GR* in other frameworks than the two extensively considered. We present here the ongoing work concerning *LLR* performed in POLAC (*Paris Observatory Lunar Analysis Center*) at SYRTE, Paris Observatory. We focus on a new generation of software that simulates the round trip time of photons from a given spacetime metric. This flexible approach allows to perform simulations in any alternative metric theories of gravity. The output of these software provides templates of anomalous residuals that should show up in real data if the underlying theory of gravity is not *GR*. Those templates can be used to give a rough estimation of the constraints on the additional parameters involved in the *Alternative Theory* (*AT*). To succeed, we are building a software which computes numerically the differential equations governing the orbital and rotational motion of bodies in the Solar System. In addition, we compute the difference $TT - TDB$ between the two time scales as partial derivatives of the solution, integrated from variational equations.

Introduction

Nowadays, *LLR* is the most accurate method to measure the Earth-Moon distance. The observable is a normal point based on several round-trip light times of photons between the emission by a *LLR* station (Fig. 1), the reflection on one of the retroreflector on Moon's surface (Fig. 2) and the detection back on Earth. These quantities are linked to the Earth-Moon distance through the use of a standard *LLR* reduction processing with an accuracy better than 1 cm.

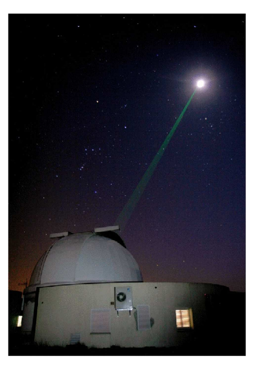

Fig. 1: *LLR* station at the Calern Observatory. France.

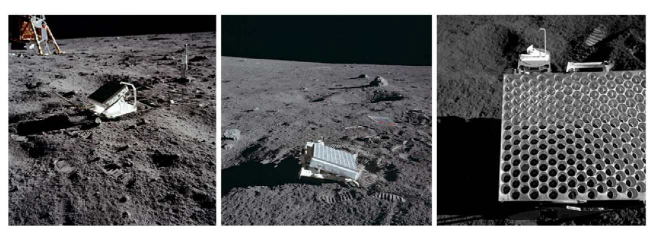

Fig. 2: Retroreflectors on the Moon's surface (Apollo 11, 14 and 15 showed in order).

Since the first "echo" in 1969 many theoretical effects have been constrained thanks to LLR's data. For instance, recent solution yields a numerical test of the *Equivalence Principle* (*EP*) comparable with the present laboratory limit at one part over 10^{13} [10]. We can refer to the same author for constraints on the *Strong Equivalence principle* (*SEP*) parameter η, *PPN* parameter of non linearity β ($= 1$ in *GR*), geodetic precession effect and $\dot{G}/G$. We can also mention the work of [8] for test of gravitomagnetism effect and the link with the preferred frame parameter α_1 appearing in the usual *PPN* framework, using *LLR* data. Finally, we refer to [7] for *LLR* analysis of the *Inverse Square Law* (*ISL*) by fitting Yukawa perturbation terms.

Main Effects

Considering the high accuracy of the *LLR* data, we have to model all dynamical effects with theoretical signal larger than 1 cm over the Earth-Moon distance. The most important are :

- ***Point-mass interactions***: we use the post-Newtonian *Eistein-Infeld-Hoffmann* (*EIH*) equations of motion in PPN framework, see e.g., [4]. The integration of the position of point-mass bodies is done in the *International Celestial Reference Frame* (*ICRF*).
- ***Figure potential***: the Moon, the Sun and the Earth are not considered as point-mass bodies. We use spherical harmonics to describe their figure potential. We expand up to degree 4 in zonal harmonic for the Earth potential, up to degree 4 in zonal, sectoral and tesseral harmonic for the Moon potential and degree 2 in zonal harmonic for the one of the Sun.
- ***Tides and spin***: we take into account distortions (due to tides and spin variation) raised upon the Earth and the Moon since they are closed to each other. These distortions induce variations in 2^{nd} degree harmonic of the two extended bodies. Subsequently, the impact on the orbital motion of point-mass body is computed with the figure potential formalism.
- ***Dissipation***: distortions are evaluated considering anelastic bodies. Since anelastic bodies don't react immediately to a perturbation, there is a time delay in their reaction because of the dissipation inside them. To consider this dissipation for tides, we introduce a phase lag between the position of a perturber and the direction of the tidal bulge. For the spin velocity vector, we consider dissipation by computing the angular velocity vector at time t minus time delay.
- ***Lunar librations***: we orientate the Moon in *ICRF* thanks to the three Euler's angles (ϕ, θ, ψ). Their evolution in time is given by Euler's equation of motion which relates the change in Moon angular velocity vector with the Moon total moment inertia tensor and its time derivative, as well as external torques acting upon the Moon.

Software

Equations of motion are integrated with the ODEX integrator [2]. In order to fit the numerical solution to real *LLR* data we perform a least squares adjustment of the initial parameters $\boldsymbol{x_0}$:

$$\boldsymbol{x} = \boldsymbol{x_0} + \boldsymbol{\delta x} = \boldsymbol{x_0} + \left\{ {}^{T}f'(\boldsymbol{x_0}) \cdot f'(\boldsymbol{x_0}) \right\}^{-1} \cdot {}^{T}f'(\boldsymbol{x_0}) \cdot \left[\boldsymbol{y} - f(\boldsymbol{x_0})\right],$$

where $\boldsymbol{y}$ represents the "range" provided by *LLR* observations and $f(\boldsymbol{x_0})$ represents the same quantity numerically integrated. $f'(\boldsymbol{x_0})$ is the partial derivative matrix, computed from the variational equation. It depends on initial values of the solution vector :

$$\boldsymbol{x_0} = {}^{T}\left(\chi^i_1, \cdots, \chi^i_{\mathcal{N}}, \zeta^i; \dot{\chi}^i_1, \cdots, \dot{\chi}^i_{\mathcal{N}}, \dot{\zeta}^i; p^l\right),$$

with $i = 1, \cdots, 3$ and $l = 1, \cdots, m$. $\boldsymbol{p}$ represents the physical parameters vector, $\boldsymbol{\chi}_{\mathrm{A}}$ the position vector of body A, $\dot{\boldsymbol{\chi}}_{\mathrm{A}}$ the velocity vector of body A, $\boldsymbol{\zeta}$ represents the three Euler's angles and $\dot{\boldsymbol{\zeta}}$ their time derivatives. Then, for $A = 1, \cdots, \mathcal{N}$; $j = 1, \cdots, 6\times(\mathcal{N}+1)+m$ and $i = 1, \cdots, 3$

$$\begin{cases} \dfrac{\mathrm{d}}{\mathrm{d}t}\left(\dfrac{\mathrm{d}\chi^i_{\mathrm{A}}}{\mathrm{d}x^j_0}\right) = \dfrac{\mathrm{d}\dot{\chi}^i_{\mathrm{A}}}{\mathrm{d}x^j_0} \\ \dfrac{\mathrm{d}}{\mathrm{d}t}\left(\dfrac{\mathrm{d}\dot{\chi}^i_{\mathrm{A}}}{\mathrm{d}x^j_0}\right) = \dfrac{\partial \mathcal{A}^i_{\mathrm{A}}}{\partial \chi^k_{\mathrm{B}}}\dfrac{\mathrm{d}\chi^k_{\mathrm{B}}}{\mathrm{d}x^j_0} + \dfrac{\partial \mathcal{A}^i_{\mathrm{A}}}{\partial \zeta^k}\dfrac{\mathrm{d}\zeta^k}{\mathrm{d}x^j_0} + \dfrac{\partial \mathcal{A}^i_{\mathrm{A}}}{\partial \dot{\chi}^k_{\mathrm{B}}}\dfrac{\mathrm{d}\dot{\chi}^k_{\mathrm{B}}}{\mathrm{d}x^j_0} + \dfrac{\partial \mathcal{A}^i_{\mathrm{A}}}{\partial \dot{\zeta}^k}\dfrac{\mathrm{d}\dot{\zeta}^k}{\mathrm{d}x^j_0} + \dfrac{\partial \mathcal{A}^i_{\mathrm{A}}}{\partial x^j_0} \end{cases}$$

where $\boldsymbol{\mathcal{A}}_{\mathrm{A}} = \ddot{\boldsymbol{\chi}}_{\mathrm{A}}(\boldsymbol{x_0})$ is the absolute acceleration vector of body A. We obtain a similar expression for $\mathrm{d}\zeta^i/\mathrm{d}x^j_0$ where $\boldsymbol{\mathcal{A}}$ is replaced by $\ddot{\boldsymbol{\zeta}}$. Red quantities are computed analytically and directly implemented into the software. The numerical computation of the $\mathrm{d}\chi^i_{\mathrm{A}}/\mathrm{d}x^j_0$ let to compute the partial derivatives matrix $f'(\boldsymbol{x_0})$. Using this semi-analytical method, we integrate the partial derivatives at the same time that the equations of motion unlike a purely numerical method.

Comparison With INPOP13c

We present a comparison between our numerical solution and INPOP13c [1]. The aim is to validate all the steps of our model implementation. Currently, the two dynamical software are close except three main differences. First of all, in our modeling, the Earth orientation is forced through the use of the IAU-routines of SOFA [9], whereas it is integrated into INPOP. Secondly, we consider the perturbation upon the Earth-Moon vector of the 70 biggest asteroids, while the effect of 300 is computed into INPOP. Finally, INPOP13c takes into account a flat ring in order to model the remaining asteroids of the main belt, which is not present in our software.

In Fig. 3, 4 and 5 we compare the two dynamical modeling by taking initial conditions (positions and velocities) of bodies and values of all physical parameters provided by INPOP13c at J2000. Then, we integrate the differential equations with our software and plot the differences between our solution and INPOP13c, over the Earth-Moon distance (c.f. Fig. 3), the 6 keplerian elements of the Moon (c.f. Fig. 4) and the three Euler's angles and their time derivatives (c.f. Fig. 5). We see that the difference is very small and lower than the accuracy of *LLR* data over the Earth-Moon distance for a timespan of 120 years centred to J2000.

The next step will be to fit our numerical solution to real *LLR* data.

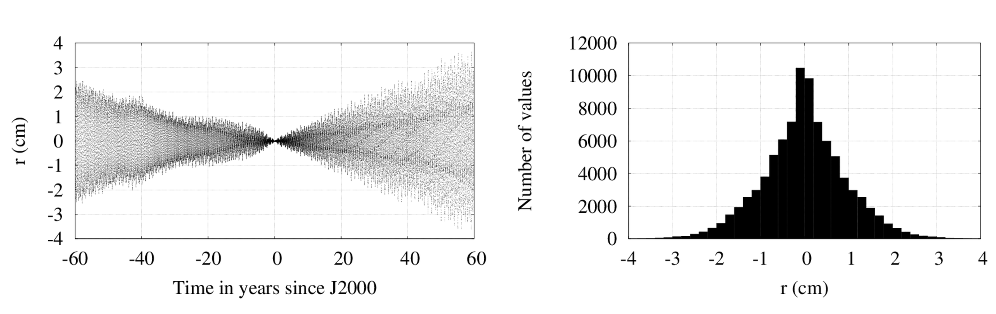

Fig. 3: Difference over the Earth Moon distance and distribution around the mean value. x axis is TDB time expressed in years since J2000.

Comparison With INPOP13c

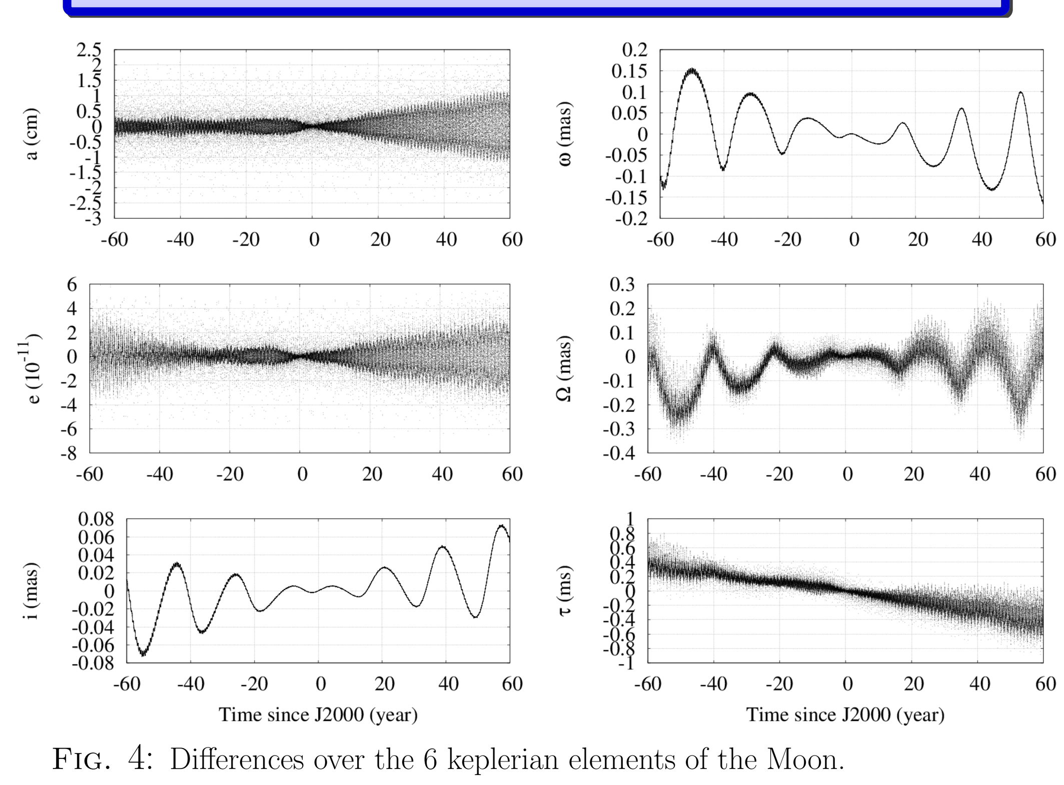

Fig. 4: Differences over the 6 keplerian elements of the Moon.

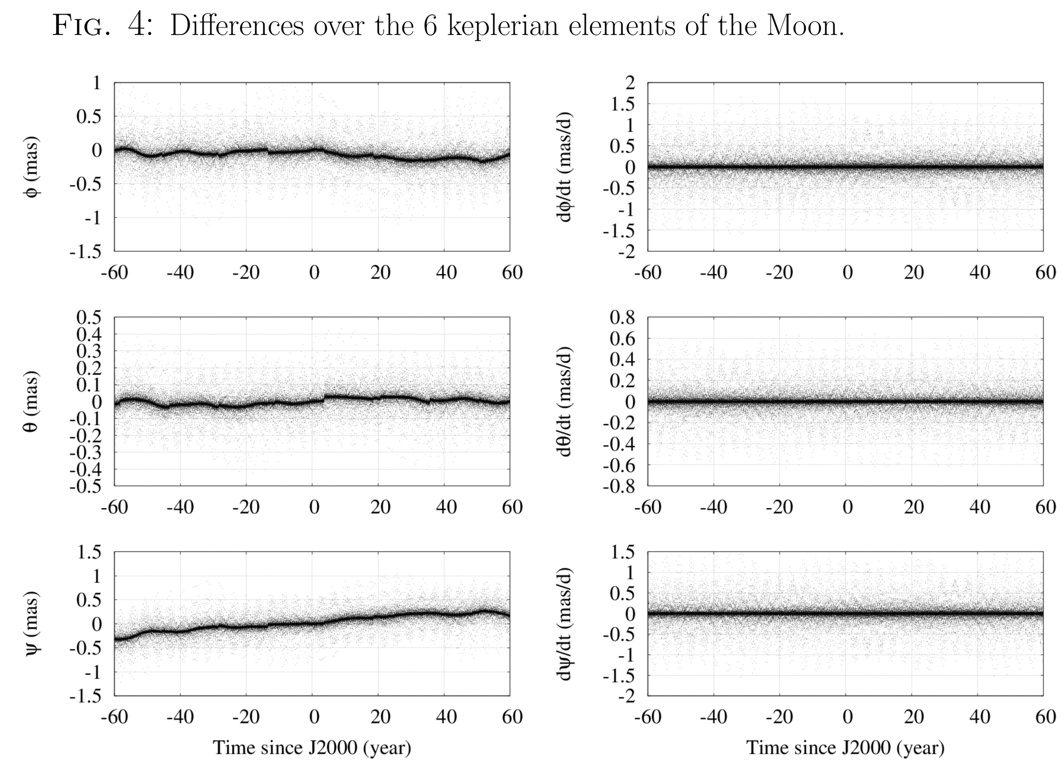

Fig. 5: Differences over the 3 Euler's angles and their time derivatives.

Bibliography

References

[1] A. Fienga, H. Manche, J. Laskar, M. Gastineau, and A. Verma. Inpop new release: Inpop13b. *ArXiv e-prints*, May 2014.

[2] E. Hairer, S. P. Norsett, and G. Wanner. *Solving Ordinary Differential Equation I. Nonstiff Problems*. Springer Series in Computational Mathematics, 1993.

[3] A. Hees, B. Lamine, S. Reynaud, M.-T. Jaekel, C. Le Poncin-Lafitte, V. Lainey, A. Füzfa, J.-M. Courty, V. Dehant, and P. Wolf. Radioscience simulations in general relativity and in alternative theories of gravity. *Classical and Quantum Gravity*, 29(23):235027, Dec. 2012.

[4] S. A. Klioner and M. H. Soffel. Relativistic celestial mechanics with ppn parameters. *Physical Review D*, 62(2):024019, July 2000.

[5] S. B. Lambert and C. Le Poncin-Lafitte. Determining the relativistic parameter γ using very long baseline interferometry. *Astronomy and Astrophysics*, 499:331–335, May 2009.

[6] S. M. Merkowitz. Tests of Gravity Using Lunar Laser Ranging. *Living Reviews in Relativity*, 13:7, Nov. 2010.

[7] J. Müller, J. G. Williams, and S. G. Turyshev. Lunar laser ranging contributions to relativity and geodesy. *ArXiv General Relativity and Quantum Cosmology e-prints*, Sept. 2005.

[8] M. Soffel, S. Klioner, J. Müller, and L. Biskupek. Gravitomagnetism and lunar laser ranging. *Physical Review*, 78(2):024033, July 2008.

[9] P. T. Wallace. Sofa: Standards of fundamental astronomy. *Highlights of Astronomy*, 11:191, 1998.

[10] J. G. Williams, S. G. Turyshev, and D. H. Boggs. Progress in Lunar Laser Ranging Tests of Relativistic Gravity. *Physical Review Letters*, 93(26):261101, Dec. 2004.